Accepted Manuscript

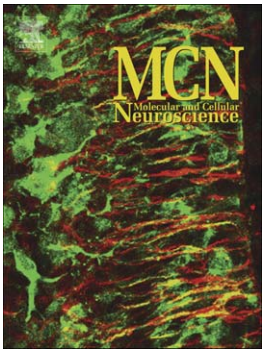

Delayed Dendritic Development in Newly Generated Dentate Granule Cells by Cell-Autonomous Expression of the Amyloid Precursor Protein

Nicolás A. Morgenstern, Damiana Giacomini, Gabriela Lombardi, Eduardo M. Castaño, Alejandro F. Schinder

PII: S1044-7431(13)00069-9
DOI: doi: 10.1016/j.mcn.2013.07.003
Reference: YMCNE 2830

To appear in: *Molecular and Cellular Neuroscience*

Received date: 5 November 2012
Revised date: 15 May 2013
Accepted date: 3 July 2013

Please cite this article as: Morgenstern, Nicolás A., Giacomini, Damiana, Lombardi, Gabriela, Castaño, Eduardo M., Schinder, Alejandro F., Delayed Dendritic Development in Newly Generated Dentate Granule Cells by Cell-Autonomous Expression of the Amyloid Precursor Protein, *Molecular and Cellular Neuroscience* (2013), doi: 10.1016/j.mcn.2013.07.003

Delayed Dendritic Development in Newly Generated Dentate Granule Cells by Cell-Autonomous Expression of the Amyloid Precursor Protein

Nicolás A. Morgenstern[*,1], Damiana Giacomini[*,1], Gabriela Lombardi[*,1], Eduardo M. Castaño[2] and Alejandro F. Schinder[1]

(*) NAM, DPG and GL contributed equally to this work.

([1]) Laboratory of Neuronal Plasticity and ([2]) Laboratory of Amyloidosis and Neurodegeneration
Leloir Institute (IIBBA-CONICET)
Buenos Aires (1405), Argentina

Corresponding author:
Alejandro F. Schinder
Laboratory of Neuronal Plasticity
Leloir Institute (IIBBA – CONICET)
Av. Patricias Argentinas 435
(1405) Buenos Aires, Argentina
Phone: +5411 5238 7500 x 3307
Fax: +5411 5238 7501
aschinder@leloir.org.ar

ABSTRACT

Neuronal connectivity and synaptic remodeling are fundamental substrates for higher brain functions. Understanding their dynamics in the mammalian allocortex emerges as a critical step to tackle the cellular basis of cognitive decline that occurs during normal aging and in neurodegenerative disorders. In this work we have designed a novel approach to assess alterations in the dynamics of functional and structural connectivity elicited by chronic cell-autonomous overexpression of the human amyloid precursor protein (hAPP). We have taken advantage of the fact that the hippocampus continuously generates new dentate granule cells (GCs) to probe morphofunctional development of GCs expressing different variants of hAPP in a healthy background. hAPP was expressed together with a fluorescent reporter in neural progenitor cells of the dentate gyrus of juvenile mice by retroviral delivery. Neuronal progeny was analyzed several days post infection (dpi). Amyloidogenic cleavage products of hAPP such as the β-C terminal fragment (β-CTF) induced a substantial reduction in glutamatergic connectivity at 21 dpi, at which time new GCs undergo active growth and synaptogenesis. Interestingly, this effect was transient, since the strength of glutamatergic inputs was normal by 35 dpi. This delay in glutamatergic synaptogenesis was paralleled by a decrease in dendritic length with no changes in spine density, consistent with a protracted dendritic development without alterations in synapse formation. Finally, similar defects in newborn GC development were observed by overexpression of α-CTF, a non-amyloidogenic cleavage product of hAPP. These results indicate that hAPP can elicit protracted dendritic development independently of the amyloidogenic processing pathway.

Keywords

Synaptogenesis – Neuronal maturation – Neurodegeneration – Dentate gyrus - Synaptic transmission

Abbreviations

CTF: C-terminal fragment of APP

Dpi: days post infection

EPSC: excitatory postsynaptic current

GC: dentate granule cell

hAPP: human Amyloid Precursor Protein

sEPSC: spontaneous excitatory postsynaptic current

INTRODUCTION

The cerebral cortex and hippocampus represent the major areas of the mammalian brain involved in higher cognitive functions. Although cortical networks exhibit highly stereotyped connectivity, these circuits undergo continuous activity-dependent synaptic remodeling (Chklovskii et al., 2004; Holtmaat et al., 2006; Knott et al., 2006). Understanding the dynamics of this process is critical to tackle the cellular basis of cognitive decline during aging or neurodegeneration. Functional changes in synaptic strength and structural modifications of the wiring diagram are two dominant types of circuit plasticity. These two forms of remodeling are closely related since potentiation and depression of preexisting neuronal connections can lead to synapse formation or elimination (Chklovskii et al., 2004; Harvey and Svoboda, 2007; Holtmaat et al., 2006; Knott et al., 2006).

Dendritic spines, the morphological correlate of excitatory synapses, can be altered in mental retardation syndromes (Comery et al., 1997; Pan et al., 2010) as well as in neurodegenerative diseases (Klapstein et al., 2001; Spires et al., 2005; Tackenberg and Brandt, 2009). Synaptic failure has been proposed as an early mechanism underlying cognitive dysfunction in Alzheimer´s disease (AD) (Selkoe, 2002). AD symptoms have been classically attributed to the deposit of amyloid beta peptide (Aβ) in the brain as amyloid plaques (Laferla and Oddo, 2005). However, since memory deficits in AD patients do not

correlate well with plaque burden, the notion that soluble monomers or oligomers of Aβ are producing early synaptic defects has emerged (Hsia et al., 1999; Lambert et al., 1998; Mucke et al., 2000). Intracerebral infusion of human Aβ oligomers or soluble Aβ derived from AD patients can reduce long-term potentiation (Shankar et al., 2007; Walsh et al., 2002), also producing behavioral deficits (Cleary et al., 2005). In addition, acute overexpression of different hAPP-related constructs in organotypic hippocampal slices was shown to depress excitatory synaptic transmission, decrease spine density and AMPA receptor number (Hsieh et al., 2006; Kamenetz et al., 2003; Shankar et al., 2007). These observations support the notion that initial stages of AD might involve failure in synaptic transmission and plasticity.

The addition of new dentate granule cells (GCs) in the adult hippocampus is a unique form of network plasticity (Mongiat and Schinder, 2011). Adult-born GCs originate from neural precursor cells that differentiate, develop, integrate and process information in a meaningful manner (Marin-Burgin et al., 2012). Thus, due to the complexity of generating an entire functional neuron in a pre-existing circuit , new neurons might be used as sensitive probes to explore specific mechanisms of morphofunctional plasticity that might be altered in neurodegenerative disorders. In the present work we utilize adult-born neurons to test the hypothesis that early impairment in AD may be consequence of subtle changes in the dynamics of cortical network remodeling, such as synapse formation, synapse elimination or dendritic growth. These synaptic alterations might be induced by proteolytic products of hAPP such as the Aβ peptide or c-terminal fragments (Sheng et al., 2012). We have analyzed morphological and functional properties of developing neurons of the dentate gyrus expressing different variants of hAPP. Interestingly, we found that different variants of hAPP induced a substantial but transient reduction of glutamatergic connectivity at 21 dpi, regardless of the presence of the amyloidogenic APP fragment. This functional alteration was paralleled by a decrease in dendritic length, consistent with a delay in dendritic growth without altering synapse formation.

MATERIAL AND METHODS

Production of viral vectors

We used a retroviral vector based on the Moloney murine leukemia virus (Laplagne et al., 2006). Retroviral particles were assembled using three separate plasmids containing the envelope (CMV-vsvg), viral proteins (CMV-gag/pol), and transgenes. Transgenes included a fluorescent reporter such as GFP or RFP, hAPP, β-CTF (both gifts from R. Malinow), or α-CTF under CAG or PGK promoters. α-CTF was obtained by deleting the first 17 aminoacids from the original β-CTF construct using standard PCR-based techniques. The primers used were: 5´ AAGCTTTACCGGGTAGGGGAGGCGCTTT 3´ (primer 1), 5´GAACACCAATGCCTGCACTGTAGCCAGG 3´ (primer 2), 5´TACAGTGCAGGCATTGGTGTTCTTTGCA3´ (primer 3) and 5´GGTTGATTGGTTTAAACAGCTCCACCGC 3´ (primer 4). The deletion was introduced via primers 2 and 3, while primers 1 and 4 were used to attach the overlap regions. The full-length deleted fragment was then subcloned to replace the β-CTF-IRES-GFP fragment by the new α-CTF-IRES-GFP. We then generated the following constructs: PGK-hAPP-IRES-GFP, PGK-β-CTF-IRES-GFP and PGK-α-CTF-IRES-GFP. Plasmids were transfected into HEK 293T cells using deacylated polyethylenimine. Virus-containing supernatant was harvested 48 h later and concentrated by two rounds of ultracentrifugation. Virus titer was typically ~10^5 particles/µl. For the coinfection experiments utilized to measure dendritic length (Fig. 5), we used a mixture of CAG-RFP and CAG-β-CTF-IRES-GFP retroviruses in a 1:2 ratio. For the coinfection experiments performed to measure neuronal survival shown in (Fig. 3), we used a mixture of CAG-RFP and CAG-β-CTF-IRES-GFP retroviruses in a 1:4 ratio. For the *in vitro* experiments and retroviral purification, HEK 293T cells were cultured in Dulbecco´s Modified Eagle´s Medium (DMEM) high glucose (pH 7.3) supplemented with 10 % FCS and 2 mM glutamine.

Subjects and stereotaxic surgery for retroviral delivery

Female C57Bl6/J mice (23–28 days old), were housed at four to five mice per cage in standard conditions. Mice were anesthetized (avertin 0.5 mg/g), and virus was infused into the right dentate gyrus (1.5 µl at 0.2 µl/min) using sterile calibrated microcapillary pipettes (Drummond Scientific) using stereotaxic surgery

[coordinates: for animals weighing below 13.5 grams -1.5 mm anteroposterior (AP), -1.5 mm lateral (L), -2.0 mm ventral (V); for >15 gram: s -1.9 mm AP, -1.7 mm L, -2 mm V]. A single injection site was sufficient to label a substantial number of neural precursor cells throughout the septotemporal axis of the hippocampus. Only neurons from the septal dentate gyrus were included in this work. Animals were killed at the indicated times [7, 21 or 35 dpi] for confocal imaging or electrophysiological recordings. Experimental protocols were approved by the Institutional Animal Care and Use Committee of the Fundación Instituto Leloir according to the Principles for Biomedical Research involving animals of the Council for International Organizations for Medical Sciences, and provisions stated in the Guide for the Care and Use of Laboratory Animals.

Electrophysiology

Mice were anesthetized (150 µg ketamine/15 µg xylazine in 10 µl of saline per g) and decapitated at 21 or 35 dpi as indicated. Brains were removed into a chilled solution containing (mM): 110 choline-Cl^-, 2.5 KCl, 2.0 NaH_2PO_4, 25 $NaHCO_3$, 0.5 $CaCl_2$, 7 $MgCl_2$, 20 dextrose, 1.3 Na^+- ascorbate, 3.1 Na^+-pyruvate, and 4 kynurenic acid. Horizontal slices (400-µm thick) were cut in a vibratome (Leica VT1200S) and transferred into a chamber containing (mM): 125 NaCl, 2.5 KCl, 2.3 NaH_2PO_4, 25 $NaHCO_3$, 2 $CaCl_2$, 1.3 $MgCl_2$, 1.3 Na^+-ascorbate, 3.1 Na^+-pyruvate, and 10 dextrose (315 mOsm). Slices were bubbled with 95% O_2/5% CO_2 and maintained at 30°C for >1 h before experiments started. Whole-cell recordings were performed at 23 ± 2°C using microelectrodes (4–6MΩ) pulled from borosilicate glass (KG-33; King Precision Glass) and filled with (mM): 120 K-gluconate, 20 KCl, 5 NaCl, 4 $MgCl_2$, 0.1 EGTA, 10 HEPES, 4 Tris-ATP, 0.3 Tris-GTP, 10 phosphocreatine, Alexa Fluor 488 or 594 (10 µg/ml; Invitrogen), pH 7.3, and 290 mOsm. Recordings were obtained using an Axopatch 200B amplifier (Molecular Devices), digitized (Digidata 1322A), and acquired at 10 and 50 kHz into a personal computer using the pClamp 9 software (Molecular Devices). Membrane capacitance (C_m) and input resistance (R_{input}) were obtained from current traces evoked by a hyperpolarizing step of 10 mV. Extracellular stimulation of the perforant path was done every 30 sec using input strength between 20 and 600 µA (50 µs) using concentric monopolar or bipolar electrodes (Frederick

Haer Company) and an Iso-Flex stimulator (AMPI). The stimulation electrode was placed in the middle third of the molecular layer anti or orthodromically from the soma of the neuron of interest. Stimulation strength was normalized using population spike: A 3 M NaCl-filled microelectrode was placed close to the soma of the target neuron; increasing stimuli (20 pA every 15 sec) were given until the extracellular response reached saturation (100%); this allowed establishing a relationship between the stimulation strength and the proportion of active axons. For the calibration of excitatory postsynaptic currents (EPSCs) stimulus strength was adjusted to provide 25, 50, 75 and 100 % of the maximal population spike. Peak EPSC amplitude was measured from the average of 4 sweeps for each stimulation intensity. In current-clamp recordings, the resting membrane potential (V_m) was kept at -80 mV by passing a holding current. Voltage-dependent Na^+ currents (I Na^+) were measured after leak subtraction using a p/6 protocol and automatic detection of the fast inward peak. Spontaneous postsynaptic excitatory currents (sEPSCs) were recorded at a holding potential of -60 mV in the presence of picrotoxin (PTX, 100 µM) and filtered at 1 kHz. Event detection was performed using the Mini Analysis software (Synaptosoft). The threshold current for spiking was assessed by successive depolarizing current steps (5 pA; 200 ms) to drive the membrane potential from resting to 0 mV. Criteria to include cells in the analysis were co-labeling with Alexa Fluor or visual confirmation of GFP in the pipette tip, and absolute leak current <50 pA at -60 mV. Series resistance was typically <25 MΩ, and experiments were discarded if >45 MΩ. Hippocampal slices with evoked population spike <1.5 mV were not considered for analysis.

Immunofluorescence

Immunostaining was done on 60 µm free floating coronal sections throughout the fixed brain. Antibodies were applied in TBS with 3% donkey serum and 0.25% Triton X-100. Double immunofluorescence was performed using the following primary antibodies: anti-GFP (rabbit polyclonal; 1:100; Invitrogen; or chicken polyclonal; 1:500; Millipore Bioscience Research Reagents; or chicken polyclonal; 1:500; Aves) and -RFP (rabbit polyclonal; 1:200; Millipore). The following corresponding secondary antibodies were used: donkey anti-rabbit Cy3 and donkey anti-chicken Cy2 (1:250; Jackson ImmunoResearch). To confirm the expression of hAPP, HEK 293T were transfected or infected (as indicated in the legend to Supplemental Fig. 1) with the

PGK-hAPP-IRES-GFP virus and subjected to western blot or immunohistochemistry assays with a specific antibody against the myc tag presented in hAPP (rabbit polyclonal 1:100; Sigma).

Confocal microscopy

Images were acquired using a Zeiss LSM 5 Pascal or a Zeiss LSM 510 Meta confocal microscopes (Carl Zeiss, Jena, Germany). For spine counts, three-dimensional reconstruction of dendritic segments was performed with the Zeiss LSM Image Browser Software from a series of 100–200 confocal planes taken at 0.1 μm intervals using a 63 x oil immersion objective as previously described (Morgenstern et al., 2008). Spine density analysis was done by manually counting spines in dendritic fragments of ~100 µm for each of 5–7 GFP^+ cells per mouse, and 3–4 mice at each time point. Only GFP^+ dendrites located in the middle third of the molecular layer were included in the analysis. For dendritic length measurements, images were acquired (40 x; NA, 1.3; oil-immersion) from 60-µm-thick sections taking *z*-series including 35–50 optical slices, airy unit = 1 at 0.8 µm intervals. The β-CTF-IRES-GFP retrovirus rendered low fluorescence intensity that was insufficient for dendritic measurements. To solve that problem, dendritic trees of β-CTF expressing neurons were characterized after coinfection with two retroviruses carrying β-CTF-IRES-GFP and CAG-RFP (Fig. 5). Dendritic length was then measured from projections of three-dimensional reconstructions onto a single plane in GCs expressing both GFP and RFP in their soma. For neuronal survival assay, P23-28 mice were coinfected with a combination of β-CTF-IRES-GFP and RFP retroviruses and animals were killed 7 or 35 days later. As a result, three populations of neurons were generated: β-CTF-GFP (green), β-CTF-GFP and RFP ("yellow"), and RFP (red) expressing neurons. Images were acquired (20 x; NA, 0.8) and the total number of green (with or without RFP) and red GCs was counted. A ratio between green over red neurons was calculated as a measure of neuronal death.

Statistical analysis

Statistics used throughout the manuscript are described in the figure legends and in the text. When data met normality tests (Gaussian distribution and equal variance), two-tailed *t* tests or ANOVA were used, as

indicated. In cases in which data did not met normality criteria, nonparametric tests were used as follows: Mann–Whitney test for independent comparisons, and Kruskal–Wallis test for multiple comparisons.

RESULTS

hAPP reduces excitatory input strength in developing GCs in the postnatal hippocampus

Network plasticity in the adult brain involves cellular mechanisms that are common to neuronal development such as dendritic remodeling, changes in synaptic strength, and synapse formation and elimination. To investigate whether these processes may be altered by hAPP, we assessed the morphofunctional development of newly generated GCs in the postnatal hippocampus after retroviral delivery of hAPP onto neural progenitor cells of the dentate gyrus. **Expression of hAPP by retroviral transduction was initially corroborated by western blot and immunohistochemistry in HEK293 cells (Supplemental Figure 1)**. To study the effects of hAPP overexpression in the development and functional integration of new GCs, three to four-week-old mice received an intrahippocampal retroviral injection to deliver the vector encoding hAPP-IRES-GFP or GFP alone (control), and neuronal phenotype was studied at 21 dpi, at which time new GCs are typically undergoing extensive dendritic growth and afferent synaptogenesis (Espósito et al., 2005). Neuronal maturation is typically finished after 40 dpi. EPSCs were then measured in whole-cell recordings from GCs in response to stimulation of the perforant path in acute slices obtained at 21 dpi (Fig. 1A). Stimuli of increasing strength evoked EPSCs of increasing amplitude. The peak amplitude for control neurons (expressing only GFP) at the strongest stimulus intensity reached ~180 pA, similarly to previous findings obtained in young adult mice (Mongiat et al., 2009). Remarkably, recordings obtained under similar conditions from GCs expressing hAPP rendered smaller EPSC amplitudes (Figure 1B-D), suggesting a reduction in afferent connectivity as a consequence of the hAPP expression that occurred throughout development of newborn GCs.

β-CTF, the amyloidogenic product of hAPP cleavage by β-secretase , has been previously shown to exert similar effects as hAPP (Hsieh et al., 2006; Kamenetz et al., 2003). Due to the smaller size of the

transgene compared to that of hAPP, a retroviral construct encoding for β-CTF allowed us to increase the efficacy of retroviral packaging, thus improving retroviral titer and transduction efficacy. We then injected a new experimental group with a retroviral vector expressing β-CTF-IRES-GFP to investigate the degree of neuronal development and connectivity at 21 dpi. GCs expressing β-CTF displayed smaller EPSC amplitude relative to control, with responses that were similar to those obtained in neurons expressing hAPP (Fig. 1B-D). The diminished amplitude of postsynaptic responses might be due to a reduced number of synaptic connections, decreased density of postsynaptic receptors (postsynaptic origin), or lower probability of neurotransmitter release (presynaptic origin). Changes in release probability are usually reflected in modifications in paired-pulse plasticity (Zucker and Regehr, 2002). Yet, paired stimulation of the perforant path elicited facilitation of postsynaptic responses of similar extent in control and β-CTF neurons, suggesting that the reduced EPSC amplitude is unlikely to be due to presynaptic differences (Fig. 2A). Recording of sEPSC revealed a lower sEPSC frequency but similar amplitude in β-CTF neurons when compared to control GCs (Fig. 2B). In light of the lack of changes in paired-pulse plasticity, these findings suggest that immature (21 dpi) GCs expressing β-CTF exhibit a lower density of synaptic inputs than control neurons.

The observed reduction in afferent connectivity might be due to a specific alteration in synapse formation or to a global impairment in the development of neurons expressing β-CTF. To refine this assessment we measured intrinsic neuronal parameters (both passive membrane properties and excitability) that reflect their overall developmental state (Espósito et al., 2005; Mongiat et al., 2009). No differences were found between control and β-CTF neurons for R_{input}, V_m or peak I Na^+ (Table 1). **The minor decrease in C_m observed for β-CTF neurons might reflect a reduction in the area of distal neuronal membrane that is better observed at the level of dendritic structure (see below).** Similar responsiveness was also observed in repetitive firing by the injection of depolarizing current steps in both neuronal populations (Fig. 2C), indicating that functional maturation is not globally affected in β-CTF neurons. Taken together, these results indicate that cell-autonomous expression of β-CTF produces specific alterations in the connectivity of developing GCs in the young adult dentate gyrus.

β-CTF does not affect neuronal survival

The altered connectivity described above might result from neurons undergoing irreversible damage, rather than from a specific defect in maturation and synaptogenesis. It is well known that during adult neurogenesis a substantial proportion of newly generated neurons undergo programmed cell death within the third week, while the remaining cells survive and become functionally integrated in the preexisting network (Dayer et al., 2003; Dupret et al., 2007; Kempermann et al., 2003). If β-CTF increased neuronal death, the survival rate of new GCs expressing β-CTF after >3 weeks should be lower than that of control newborn GCs expressing only a fluorescent marker. Thus, neural progenitor cells of the dentate gyrus were transduced simultaneously with two retroviruses encoding β-CTF-IRES-GFP and RFP (control), respectively. We then counted control (red) and β-CTF neurons (green) at early (7 dpi) and late time points (35 dpi) to determine whether the proportion of β-CTF neurons (green) / control (red) cells was similar or different at 7 vs. 35 dpi. Interestingly, the proportion of β-CTF neurons at 35 dpi was similar to that observed at 7 dpi (Fig. 3C), indicating that the observed reduction in the afferent connectivity of β-CTF neurons is not due to a decreased neuronal survival.

β-CTF produces a delay in functional and morphological maturation in newborn GCs

To determine whether the altered connectivity induced by β-CTF is persistent, we performed whole-cell recordings at 35 dpi. Remarkably, both control and β-CTF populations displayed more mature functional characteristics than those observed at 21 dpi, as revealed by EPSC amplitude, firing of action potentials, and passive membrane properties (Fig. 4 and Table 1). No significant differences were found between control and β-CTF GC populations, indicating that connectivity defects observed at 21 dpi are completely reverted by 35 days. In summary, β-CTF overexpression produces a transient delay in GC development that is primarily reflected in afferent synaptogenesis.

Dendritic spines are the structural correlates of glutamatergic synapses. Our electrophysiological findings suggest that β-CTF produces a delay in glutamatergic synaptogenesis in new GCs. The smaller

number of functional glutamatergic synapses observed at 21 dpi as compared to control GCs might reflect a reduction in the total number of afferent synapses at that developmental stage, or to a proportion of synaptic contacts that are structurally formed but functionally impaired. To better understand this phenomenon we performed confocal images of hippocampal sections bearing control and β-CTF neurons at 21 and 35 dpi. Dendritic spine density was found to be similar for both neuronal populations at 21 dpi (Fig. 5A,C). However, the total length of the dendritic tree was significantly shorter in β-CTF neurons (Fig. 5B,D). Dendritic length was reduced by ~30 %, which represents a reliable morphological correlate to the observed reduction in evoked EPSC amplitude and it is also consistent with the slight decrease in C_m (Table 1). In contrast, neuronal morphology at 35 dpi displayed similar features in control and β-CTF GCs (Fig. 5E-H), in agreement with our electrophysiological results obtained at that neuronal age. Therefore, β-CTF overexpression induces a transient deficit in connectivity that recovers completely by 35 days.

The reduced connectivity of developing GCs is independent of β-amyloid production

The processing of hAPP involves two alternative pathways: 1) β-secretase gives rise to β-CTF that, in turn, generates β amyloid peptide after cleavage by γ-secretase; 2) α-secretase gives rise to α-CTF that then generates the non-amyloidogenic "p3" peptide after γ-secretase cleavage (Sheng et al., 2012). To test whether the effects observed by the overexpression of hAPP and β-CTF are related to the amyloidogenic cleavage pathway, a new retroviral construct was designed to overexpress α-CTF. Electrophysiological recordings were then performed in 21 dpi neurons. Stimulation of the perforant path elicited EPSCs of smaller amplitude in neurons expressing α-CTF when compared with control cells (Fig. 6A), similarly to what we observed in β-CTF neurons. This effect appears to be primarily due to afferent connectivity since intrinsic membrane properties have remained in general unaltered (Fig. 6B and Table 1). **In addition, analysis of sEPSCs in α-CTF neurons revealed similar amplitude but a somehow reduced frequency, consistent with a decrease in the total number of synapses (Fig. 6C). Indeed, morphological analysis revealed a shortened dendritic tree in α-CTF neurons when compared to RFP-expressing controls, which is consistent with a reduced density of afferent synaptic connectivity (Fig. 6D).** Altogether, these data

indicates that hAPP and its variants produce a significant delay in dendritic remodeling that is unrelated to amyloidogenic effects.

DISCUSSION

Intensive investigation has led to the idea that APP (particularly its proteolytic products) may be responsible for alterations in synaptic transmission and plasticity that occur in different models of AD (Sheng et al., 2012). Yet, the question of whether APP alters synapse formation has not been approached. To address this specific problem we have taken advantage of the fact that the dentate gyrus of the hippocampus generates neurons through life, starting from undifferentiated neural progenitor cells that must establish all synaptic connections de novo (Piatti et al., 2006; Zhao et al., 2008). Thus, chronic single-cell overexpression of different variants of APP in neural progenitor cells allowed us to assess possible morphofunctional alterations in developing GCs in an otherwise healthy background. We found that chronic APP expression induces a functional and structural delay in the development of afferent synaptic connectivity and, consequently, functional integration of new GCs. Furthermore, combining this approach with different variants of APP we have concluded that both the amyloidogenic and non-amyloidogenic forms β-CTF and α-CTF affect neuronal plasticity in a remarkably similar fashion. The delay in the establishment of functional inputs is a consequence of an altered dendritic growth rather than in synapse formation. This conclusion is supported by the findings that: 1) at 21 dpi the reduction in the amplitude of evoked EPSCs by APP variants is paralleled by a decrease in the frequency but not the amplitude of spontaneous synaptic events; 2) β-CTF **and α-CTF** neurons at 21 dpi display shorter dendrites but no differences in spine density when compared to control GCs of the same age; 3) the extent of dendritic tree shortening predicts a decrease in the number of synapses that is compatible with the reduction in EPSC amplitude. We therefore provide in vivo evidence for a reduction in neuronal connectivity produced by chronic actions of APP and its proteolytic derivatives.

Previous works using transgenic animals to overexpress mutant forms of APP have revealed impairment in synaptic transmission and morphology that parallel behavioral deficits (Hsia et al., 1999;

Mucke et al., 2000; Spires and Hyman, 2005; Spires et al., 2005; Stern et al., 2004). In most transgenic models APP overexpression is global (not restricted to specific neuronal populations) and yet synaptic alterations were limited, even when observed in aged animals with a large burden of amyloid plaque deposition. It has also been proposed that early cognitive decline might be consequence of soluble forms of Aβ acting on synapses long time before plaque consolidation. Consistent with this hypothesis, natural Aβ oligomers derived from AD patient brains delivered onto organotypic hippocampal cultures were found to decrease the density of dendritic spines, functional active synapses and impair synaptic plasticity and memory (Shankar et al., 2007; Shankar et al., 2008). The possibility that Aβ might produce early synaptic defects independently of plaque formation was also supported by experiments using overexpression of APP and related constructs using sindbis virus in organotypic hippocampal cultures. CA1 hippocampal neurons overexpressing APP for about one day displayed substantial synaptic depression and decreased spine density (Hsieh et al., 2006; Kamenetz et al., 2003). This effect was not limited to cell autonomous mechanisms, since synapses that are located in the vicinity (within 10 μm) of APP expressing neurites did also display alterations (Wei et al., 2010). Taken together, these studies have argued in favor of early synaptic defects that would not require amyloid plaque formation.

Our observation that single-cell overexpression of APP derivatives produce transient effects in dendritic growth (in particular, hAPP and β-CTF), might in principle seem contradictory to the results discussed above describing more profound functional and morphological synaptic alterations. However, experimental variations among these studies might largely contribute to the observed differences. First, here we use a retroviral expression system that induces chronic transgene expression at low levels (typically, a single copy of the transgene is incorporated in the neuronal genome), and the effects are evaluated several weeks later. In contrast, the experiments conducted using sindbis virus (Hsieh et al., 2006; Kamenetz et al., 2003; Wei et al., 2010) or acute infusion of Aβ oligomers (Shankar et al., 2007; Shankar et al., 2008) characterize short-term effects elicited by high-expression systems or direct delivery onto brain slices, whose transient or persistent nature cannot be distinguished due to limitations in the experimental approach. Likewise, our long-term in vivo approach could mask reversible effects that occur at fast time scales. Second, neurons receiving insults in vitro might be in a more sensitive condition that

facilitates a pathological response compared to those neurons that receive comparable insults in the context of a healthy brain. Finally, it should be taken into account that those short-term studies focus on pyramidal cells, whereas this work is concentrated in newly generated dentate granule cells, which might exhibit different sensitivity to the insult.

The similarity in the effects elicited by α- and β-CTF strongly suggests that the altered dendritic growth observed here is independent of the amyloidogenic capacity of hAPP. **In principle, these effects might be related to the physiological roles of APP in neuronal development that have been recently found. In fact APP has been shown to interact with G proteins and with alpha- and beta-integrins, both in the context of processes that regulate dendritic or axonal growth in developing neurons (Billnitzer et al., 2013; Deyts et al., 2012; Hoe et al., 2009; Rama et al., 2012). Since dendritic, axonal and synaptic remodeling occur throughout life in several brain structures including the cortex and hippocampus, it is likely that the underlying mechanisms of plasticity processes that take place in the adult brain share signaling components that are common to development and plasticity.**

In recent years it has been proposed that multiple factors other than Aβ might contribute to the pathogenesis of AD (Pimplikar et al., 2010; Sheng et al., 2012). For instance p3, the γ-secretase cleavage product of α-CTF (also known as Aβ17-42), has also been implicated in neuronal dysfunction, although it has not been studied as intensively as the Aβ peptide. P3 peptides form ion channel that misbalance calcium homeostasis and lead to neurite degeneration in cultured human cortical neurons (Jang et al., 2010). This peptide has also been implicated in neuronal apoptosis through the activation of JNK and caspase-8 pathways (Wei et al., 2002). Our results might be in agreement with those alternative hypotheses that factors other than Aβ1-42 may also contribute to neuronal dysfunction and neurodegeneration.

In the rodent hippocampus, adult neurogenesis decreases with aging (Kempermann et al., 1998; Kuhn et al., 1996; Morgenstern et al., 2008). This reduction in the number of newborn neurons was proposed to underlie cognitive deficits related to senescence. In humans, it would also be feasible that increased neuronal death during AD provoked mild cognitive decline found in the pathology, provided

neurogenesis occurred in significant amounts at advanced ages, which remains unknown for the human brain. Consistent with this idea, transgenic models of AD had shown alterations in long-term survival of newborn neurons (Verret et al., 2007) and also mild delays in neuronal maturation (Li et al., 2009). Interestingly, altered development of adult-born neurons was also found in the J20 transgenic mouse (Sun et al., 2009). However, in addition to the enhanced Aβ production, the J20 mouse also displays a substantial degree of hyperexcitability that might by itself provoke profound alterations in neuronal development (Jakubs et al., 2006; Jessberger et al., 2007). In the present work, we examined if single-cell expression of β-CTF reduced neuronal survival. **We compared the proportion of β-CTF expressing neurons (relative to control) at 7 or 35 dpi and found no changes in long-term survival. This result suggests that the reduced dendritic length observed at 21 dpi was not a consequence of halted dendritic growth due to neuronal death but, instead, it was due to a specific delay in dendritic maturation.**

Neuronal connectivity and synaptic remodeling are fundamental substrates for higher brain functions both in the young adult and aging brain. Cortical circuits undergo continuous activity-dependent remodeling (Chklovskii et al., 2004; Knott et al., 2006). Such network remodeling involves both functional changes in the strength of pre-existing synapses (such as long-term potentiation and depression), and structural changes in the wiring diagram such as formation of new synapses and elimination of preexisting ones. The emerging model is that structural remodeling has a key role in experience-dependent modification in cortical networks (Chklovskii et al., 2004; Harvey and Svoboda, 2007). In this context, the delay in dendritic growth and concomitant afferent synaptogenesis observed here reveal a neuronal substrate with impaired plasticity, which might contribute to the APP-related alterations observed in AD.

CONCLUSIONS

We have utilized a novel approach to reveal cellular defects associated to early neurodegenerative dysfunctions. This approach allows discriminating cell-autonomous versus global effects of protein overexpression in vivo. We have transduced candidate transgenes related to AD to study their effect on

neuronal growth and synaptogenesis. We found transient functional and morphological delay in newborn neuron development. Since these new GCs are a very robust cell type and exhibit unique plasticity features, the observation that they are affected by overexpression of hAPP derivatives strongly suggests that neurons **in aged animals** might be even more susceptible to insults. This phenomenon might reduce global circuit plasticity which could be, at least in part, responsible for early cognitive alterations found during initial stages of AD.

ACKNOWLEDGEMENTS

We thank Mariela Veggetti for technical assistance and Maxi Neme for help with confocal microscopy. We thank R. Malinow for kindly providing the hAPP-IRES-GFP and β-CTF-IRES-GFP constructs. A.F.S. and E.M.C. are investigators of the Argentine National Research Council (Consejo Nacional de Investigaciones Científicas y Técnicas - CONICET). N.A.M., D.P.G. and G.L. were supported by fellowships from CONICET. This work was supported by the Guggenheim Foundation Fellowship and by grants from the Agencia Nacional para la Promoción de Ciencia y Tecnología (PICT2008), the American Health Assistance Foundation (Alzheimer's Disease Research grant #A2007-078), the Delfina Baratelli Foundation, and the Howard Hughes Medical Institute (International Scholars Program, grant # 55005963) to A.F.S.

REFERENCES

Billnitzer, A.J., Barskaya, I., Yin, C., Perez, R.G., 2013. APP independent and dependent effects on neurite outgrowth are modulated by the receptor associated protein (RAP). J Neurochem 124, 123-132.

Cleary, J.P., Walsh, D.M., Hofmeister, J.J., Shankar, G.M., Kuskowski, M.A., Selkoe, D.J., Ashe, K.H., 2005. Natural oligomers of the amyloid-beta protein specifically disrupt cognitive function. Nat.Neurosci. 8, 79-84.

Comery, T.A., Harris, J.B., Willems, P.J., Oostra, B.A., Irwin, S.A., Weiler, I.J., Greenough, W.T., 1997. Abnormal dendritic spines in fragile X knockout mice: maturation and pruning deficits. Proc Natl Acad Sci U S A 94, 5401-5404.

Chklovskii, D.B., Mel, B.W., Svoboda, K., 2004. Cortical rewiring and information storage. Nature 431, 782-788.

Dayer, A.G., Ford, A.A., Cleaver, K.M., Yassaee, M., Cameron, H.A., 2003. Short-term and long-term survival of new neurons in the rat dentate gyrus. J.Comp Neurol. 460, 563-572.

Deyts, C., Vetrivel, K.S., Das, S., Shepherd, Y.M., Dupre, D.J., Thinakaran, G., Parent, A.T., 2012. Novel GalphaS-protein signaling associated with membrane-tethered amyloid precursor protein intracellular domain. J Neurosci 32, 1714-1729.

Dupret, D., Fabre, A., Dobrossy, M.D., Panatier, A., Rodriguez, J.J., Lamarque, S., Lemaire, V., Oliet, S.H., Piazza, P.V., Abrous, D.N., 2007. Spatial learning depends on both the addition and removal of new hippocampal neurons. PLoS.Biol. 5, e214.

Espósito, M.S., Piatti, V.C., Laplagne, D.A., Morgenstern, N.A., Ferrari, C.C., Pitossi, F.J., Schinder, A.F., 2005. Neuronal differentiation in the adult hippocampus recapitulates embryonic development. J.Neurosci. 25, 10074-10086.

Harvey, C.D., Svoboda, K., 2007. Locally dynamic synaptic learning rules in pyramidal neuron dendrites. Nature 450, 1195-1200.

Hoe, H.S., Lee, K.J., Carney, R.S., Lee, J., Markova, A., Lee, J.Y., Howell, B.W., Hyman, B.T., Pak, D.T., Bu, G., Rebeck, G.W., 2009. Interaction of reelin with amyloid precursor protein promotes neurite outgrowth. J Neurosci 29, 7459-7473.

Holtmaat, A., Wilbrecht, L., Knott, G.W., Welker, E., Svoboda, K., 2006. Experience-dependent and cell-type-specific spine growth in the neocortex. Nature 441, 979-983.

Hsia, A.Y., Masliah, E., McConlogue, L., Yu, G.Q., Tatsuno, G., Hu, K., Kholodenko, D., Malenka, R.C., Nicoll, R.A., Mucke, L., 1999. Plaque-independent disruption of neural circuits in Alzheimer's disease mouse models. Proc.Natl.Acad.Sci.U.S.A 96, 3228-3233.

Hsieh, H., Boehm, J., Sato, C., Iwatsubo, T., Tomita, T., Sisodia, S., Malinow, R., 2006. AMPAR removal underlies Abeta-induced synaptic depression and dendritic spine loss. Neuron 52, 831-843.

Jakubs, K., Nanobashvili, A., Bonde, S., Ekdahl, C.T., Kokaia, Z., Kokaia, M., Lindvall, O., 2006. Environment matters: synaptic properties of neurons born in the epileptic adult brain develop to reduce excitability. Neuron 52, 1047-1059.

Jang, H., Arce, F.T., Ramachandran, S., Capone, R., Azimova, R., Kagan, B.L., Nussinov, R., Lal, R., 2010. Truncated beta-amyloid peptide channels provide an alternative mechanism for Alzheimer's Disease and Down syndrome. Proc Natl Acad Sci U S A 107, 6538-6543.

Jessberger, S., Zhao, C., Toni, N., Clemenson, G.D., Jr., Li, Y., Gage, F.H., 2007. Seizure-associated, aberrant neurogenesis in adult rats characterized with retrovirus-mediated cell labeling. J Neurosci 27, 9400-9407.

Kamenetz, F., Tomita, T., Hsieh, H., Seabrook, G., Borchelt, D., Iwatsubo, T., Sisodia, S., Malinow, R., 2003. APP processing and synaptic function. Neuron 37, 925-937.

Kempermann, G., Gast, D., Kronenberg, G., Yamaguchi, M., Gage, F.H., 2003. Early determination and long-term persistence of adult-generated new neurons in the hippocampus of mice. Development 130, 391-399.

Kempermann, G., Kuhn, H.G., Gage, F.H., 1998. Experience-induced neurogenesis in the senescent dentate gyrus. J.Neurosci. 18, 3206-3212.

Klapstein, G.J., Fisher, R.S., Zanjani, H., Cepeda, C., Jokel, E.S., Chesselet, M.F., Levine, M.S., 2001. Electrophysiological and morphological changes in striatal spiny neurons in R6/2 Huntington's disease transgenic mice. J Neurophysiol 86, 2667-2677.

Knott, G.W., Holtmaat, A., Wilbrecht, L., Welker, E., Svoboda, K., 2006. Spine growth precedes synapse formation in the adult neocortex in vivo. Nat.Neurosci. 9, 1117-1124.

Kuhn, H.G., Dickinson-Anson, H., Gage, F.H., 1996. Neurogenesis in the dentate gyrus of the adult rat: age-related decrease of neuronal progenitor proliferation. J.Neurosci. 16, 2027-2033.

Laferla, F.M., Oddo, S., 2005. Alzheimer's disease: Abeta, tau and synaptic dysfunction. Trends Mol.Med. 11, 170-176.

Lambert, M.P., Barlow, A.K., Chromy, B.A., Edwards, C., Freed, R., Liosatos, M., Morgan, T.E., Rozovsky, I., Trommer, B., Viola, K.L., Wals, P., Zhang, C., Finch, C.E., Krafft, G.A., Klein, W.L., 1998. Diffusible, nonfibrillar ligands derived from Abeta1-42 are potent central nervous system neurotoxins. Proc.Natl.Acad.Sci.U.S.A 95, 6448-6453.

Laplagne, D.A., Espósito, M.S., Piatti, V.C., Morgenstern, N.A., Zhao, C., van Praag, H., Gage, F.H., Schinder, A.F., 2006. Functional convergence of neurons generated in the developing and adult hippocampus. PLoS.Biol. 4, e409.

Li, G., Bien-Ly, N., Andrews-Zwilling, Y., Xu, Q., Bernardo, A., Ring, K., Halabisky, B., Deng, C., Mahley, R.W., Huang, Y., 2009. GABAergic interneuron dysfunction impairs hippocampal neurogenesis in adult apolipoprotein E4 knockin mice. Cell Stem Cell 5, 634-645.

Marin-Burgin, A., Mongiat, L.A., Pardi, M.B., Schinder, A.F., 2012. Unique processing during a period of high excitation/inhibition balance in adult-born neurons. Science 335, 1238-1242.

Mongiat, L.A., Espósito, M.S., Lombardi, G., Schinder, A.F., 2009. Reliable activation of immature neurons in the adult hippocampus. PLoS.ONE. 4, e5320.

Mongiat, L.A., Schinder, A.F., 2011. Adult neurogenesis and the plasticity of the dentate gyrus network. Eur J Neurosci 33, 1055-1061.

Morgenstern, N.A., Lombardi, G., Schinder, A.F., 2008. Newborn granule cells in the ageing dentate gyrus. J.Physiol 586, 3751-3757.

Mucke, L., Masliah, E., Yu, G.Q., Mallory, M., Rockenstein, E.M., Tatsuno, G., Hu, K., Kholodenko, D., Johnson-Wood, K., McConlogue, L., 2000. High-level neuronal expression of abeta 1-42 in wild-type human amyloid protein precursor transgenic mice: synaptotoxicity without plaque formation. J.Neurosci. 20, 4050-4058.

Pan, F., Aldridge, G.M., Greenough, W.T., Gan, W.B., 2010. Dendritic spine instability and insensitivity to modulation by sensory experience in a mouse model of fragile X syndrome. Proc Natl Acad Sci U S A 107, 17768-17773.

Piatti, V.C., Esposito, M.S., Schinder, A.F., 2006. The timing of neuronal development in adult hippocampal neurogenesis. Neuroscientist. 12, 463-468.

Pimplikar, S.W., Nixon, R.A., Robakis, N.K., Shen, J., Tsai, L.H., 2010. Amyloid-independent mechanisms in Alzheimer's disease pathogenesis. J Neurosci 30, 14946-14954.

Rama, N., Goldschneider, D., Corset, V., Lambert, J., Pays, L., Mehlen, P., 2012. Amyloid precursor protein regulates netrin-1-mediated commissural axon outgrowth. J Biol Chem 287, 30014-30023.

Selkoe, D.J., 2002. Alzheimer's disease is a synaptic failure. Science 298, 789-791.

Shankar, G.M., Bloodgood, B.L., Townsend, M., Walsh, D.M., Selkoe, D.J., Sabatini, B.L., 2007. Natural oligomers of the Alzheimer amyloid-beta protein induce reversible synapse loss by modulating an NMDA-type glutamate receptor-dependent signaling pathway. J Neurosci 27, 2866-2875.

Shankar, G.M., Li, S., Mehta, T.H., Garcia-Munoz, A., Shepardson, N.E., Smith, I., Brett, F.M., Farrell, M.A., Rowan, M.J., Lemere, C.A., Regan, C.M., Walsh, D.M., Sabatini, B.L., Selkoe, D.J., 2008. Amyloid-beta protein dimers isolated directly from Alzheimer's brains impair synaptic plasticity and memory. Nat.Med. 14, 837-842.

Sheng, M., Sabatini, B.L., Sudhof, T.C., 2012. Synapses and Alzheimer's disease. Cold Spring Harb Perspect Biol 4.

Spires, T.L., Hyman, B.T., 2005. Transgenic models of Alzheimer's disease: learning from animals. NeuroRx 2, 423-437.

Spires, T.L., Meyer-Luehmann, M., Stern, E.A., McLean, P.J., Skoch, J., Nguyen, P.T., Bacskai, B.J., Hyman, B.T., 2005. Dendritic spine abnormalities in amyloid precursor protein transgenic mice demonstrated by gene transfer and intravital multiphoton microscopy. J.Neurosci. 25, 7278-7287.

Stern, E.A., Bacskai, B.J., Hickey, G.A., Attenello, F.J., Lombardo, J.A., Hyman, B.T., 2004. Cortical synaptic integration in vivo is disrupted by amyloid-beta plaques. J Neurosci 24, 4535-4540.

Sun, B., Halabisky, B., Zhou, Y., Palop, J.J., Yu, G., Mucke, L., Gan, L., 2009. Imbalance between GABAergic and Glutamatergic Transmission Impairs Adult Neurogenesis in an Animal Model of Alzheimer's Disease. Cell Stem Cell 5, 624-633.

Tackenberg, C., Brandt, R., 2009. Divergent pathways mediate spine alterations and cell death induced by amyloid-beta, wild-type tau, and R406W tau. J Neurosci 29, 14439-14450.

Verret, L., Jankowsky, J.L., Xu, G.M., Borchelt, D.R., Rampon, C., 2007. Alzheimer's-type amyloidosis in transgenic mice impairs survival of newborn neurons derived from adult hippocampal neurogenesis. J Neurosci 27, 6771-6780.

Walsh, D.M., Klyubin, I., Fadeeva, J.V., Cullen, W.K., Anwyl, R., Wolfe, M.S., Rowan, M.J., Selkoe, D.J., 2002. Naturally secreted oligomers of amyloid beta protein potently inhibit hippocampal long-term potentiation in vivo. Nature 416, 535-539.

Wei, W., Nguyen, L.N., Kessels, H.W., Hagiwara, H., Sisodia, S., Malinow, R., 2010. Amyloid beta from axons and dendrites reduces local spine number and plasticity. Nat Neurosci 13, 190-196.

Wei, W., Norton, D.D., Wang, X., Kusiak, J.W., 2002. Abeta 17-42 in Alzheimer's disease activates JNK and caspase-8 leading to neuronal apoptosis. Brain 125, 2036-2043.

Zhao, C., Deng, W., Gage, F.H., 2008. Mechanisms and functional implications of adult neurogenesis. Cell 132, 645-660.

Zucker, R.S., Regehr, W.G., 2002. Short-term synaptic plasticity. Annu Rev Physiol 64, 355-405.

FIGURE LEGENDS

Figure 1. Retroviral expression of hAPP variants decreases input strength in three-week old GCs. ***A*,** Schematic representation of perforant path stimulation during whole-cell recording of 21 dpi newborn GCs; mPP: medial perforant path. ***B***, Example traces of excitatory postsynaptic currents (EPSCs) elicited by stimulation of the perforant path at increasing strengths in control (black), hAPP (red) or β-CTF (blue) expressing GCs. EPSCs were recorded at a holding potential of -60 mV in the presence of 100 µM PTX. Calibration: 50 pA, 10 ms. ***C***, Peak EPSC amplitudes elicited by increasing stimulus strengths for control (n=23), hAPP (n=10), and β-CTF (n=13) expressing GCs. ***D***, Peak EPSC amplitudes measured for 100 % stimulus strength. Significant differences were found among **control and β-CTF** population means (p<0.05, one way ANOVA).

Figure 2. Reduced number of glutamatergic synapses in 21 dpi GCs expressing β-CTF. ***A***, Paired stimulation (50 ms inter-pulse interval) of the perforant path elicits EPSC facilitation in control and β-CTF neurons. Scale bars: 50 pA (control) or 20 pA (β-CTF), 20 ms. Facilitation ratios are shown in the right panel. Bars represent mean ± SEM, with n = 19 (control) and n = 13 (β-CTF); p = 0.89 (Mann–Whitney's test). ***B***, Spontaneous postsynaptic current (sEPSCs) recordings obtained from control or β-CTF neurons held at -60 mV. Scale bars: 10 pA, 5 s. sEPSC frequency and amplitude are shown in the lower panels. (**) denotes p = 0.035 (Mann–Whitney's test; p = 0.96 for Amplitude values). Bars represent mean ± SEM, with n = 17 (control) and n = 12 (β-CTF). ***C***. Representative traces showing repetitive spiking in response to depolarizing current steps (step = 30 pA, 200 ms) in newborn GCs. Scale bars: 100 mV, 100 ms. The right panel shows the number of spikes evoked by increasing current steps, with n = 23 (control) and n = 14 (β-CTF).

Figure 3. β-CTF does not affect survival of new GCs. ***A***, Experimental design: a mixture of β-CTF-GFP and RFP-expressing retroviruses was injected into the dentate gyrus of mice (day 0) to label dividing progenitor cells with either vector or both together. The numbers of β-CTF expressing GCs (GFP^+) and control

newborn cells (RFP^+) were counted at 7 and 35 dpi, and the ratios GFP^+/RFP^+ cells were calculated. Neurons expressing both markers ("yellow") were considered as part of the β-CTF (GFP^+) population. ***B***, Representative confocal images displaying GCs expressing GFP (β-CTF, green), RFP (control, red) or both (yellow) at 7 and 35 dpi. The granule cell layer has been labeled using DAPI (gray). Scale bar: 50 µm. ML: molecular layer; GCL: granule cell layer; H: hilus. ***C***, Relative survival, measured as the proportion of β-CTF/control neurons normalized to the ratio obtained at 7 dpi, with n = 1244 cells from 6 animals (7 dpi) and 581 cells from 6 animals (35 dpi); $p = 0.43$, Student's *t*-test. Bars represent mean ± SEM.

Figure 4. Afferent connectivity in β-CTF neurons is restored at 35 dpi. ***A***, EPSC recordings elicited by perforant path stimulation at increasing strengths in control (black) or β-CTF (blue) neurons at 35 dpi. Scale bars: 50 pA, 10 ms. Peak EPSC amplitudes elicited by increasing stimulus strengths (right panel). ***B***, Representative traces showing repetitive spikes. Scale bars: 100 mV, 100 ms. The right panel shows the number of spikes evoked by increasing current steps, with n = 17 (control) and n = 9 (β-CTF).

Figure 5. Delayed dendritic development in GCs expressing β-CTF. ***A***, Representative confocal images of spiny dendrites from control and β-CTF GCs at 21 dpi. Scale bars: 5 µm. ***B***, Confocal images displaying control and β-CTF GCs at 21 dpi. The granule cell layer has been labeled with DAPI. Insets show colocalization of RFP and GFP in the soma of coinfected neurons. Scale bars: 40 µm. ***C***, Spine density at 21 dpi, with n = 19 (control, total measured length = 1275 µm) and n = 15 (β-CTF, total measured length = 1040 µm); $p = 0.82$ with Mann–Whitney´s test. ***D***, Dendritic length at 21 dpi. n = 15 GCs for each condition, control and β-CTF . (***) denotes $p = 0.0007$ after Mann–Whitney's test. ***E***,***F***, Representative confocal images of spiny dendrites (**E**) and entire neurons (**F**) from control and β-CTF GCs at 35 dpi. Scale bars: 5 µm (E) and 40 µm (F). ***G***, Spine density at 35 dpi, with n = 13 (control, total measured length = 1880 µm) and n = 12 (β-CTF, total measured length = 1375 µm); $p = 0.16$ with Mann–Whitney´s test. ***H***, Dendritic length at 35 dpi. n = 27-31 GCs for each condition.

Figure 6. Reduction of EPSC amplitude and dendritic development in 21 dpi GCs expressing a non-amyloidogenic fragment of hAPP. ***A***, Example EPSC recordings (holding potential -60 mV, +100 µM PTX) elicited by stimulation of the perforant path at increasing strengths in control (black) or α-CTF (green) neurons. Calibration: 50 pA, 10 ms. The right panel shows peak EPSC amplitudes vs. stimulus strength for control (n=23) and α-CTF (n=7). (*) denotes $p < 0.05$ by two-way ANOVA followed by Bonferroni´s post hoc test. ***B***, Representative traces showing repetitive spiking in response to depolarizing current steps in newborn GCs. Scale bars: 100 mV, 100 ms. The right panel shows the number of spikes evoked by increasing current steps, with n = 17 (control) and n = 9 (α-CTF). ***C***, Quantification of sEPSCs obtained from control or α -CTF neurons held at -60 mV. sEPSC amplitude and frequency are shown, with $p = 0.26$ (Amplitude) and $p = 0.20$ (Frequency); Mann–Whitney's test. Bars represent mean ± SEM, with n = 17 (control) and n = 6 (α-CTF). ***D***, *left panel,* confocal image displaying an example of α-CTF GC. Insets show colocalization of RFP and GFP in the soma. Scale bar: 40 µm. *Right panel*, dendritic length, with n = 15 GCs (control) and n = 39 (α-CTF). (***) denotes $p < 0.0001$, Mann–Whitney's test.

Table 1. Membrane properties of control and CTF-expressing neurons at different developmental stages

Values denote mean ± SEM, with cell numbers in parentheses. Statistical analysis was performed using ANOVA followed by post hoc Bonferroni's test (21 dpi) or *t*-test (35 dpi). (*) denotes $p < 0.01$ for both comparisons (α-CTF vs. control and β-CTF). Note that C_m is slightly smaller than controls for both for α- and β-CTF-expressing neurons.

Supplemental Figure 1. Detection of hAPP expression in HEK 293T cells. ***A***, Western blot of HEK 293T cells transfected with the vector PGK-hAPP-IRES-GFP (hAPP-myc tagged) (lanes 1 and 2) or PGK-GFP (lanes 3 and 4). Samples were assayed in duplicate. Lysates of untransfected cells were used as negative control (lane 5). α-actin was used as loading control. ***B***, HEK 293T cells infected with a retrovirus encoding for hAPP and GFP (hAPP-myc tagged) or GFP only. After 48hs cells were fixed and immunostained with antibodies for myc

and GFP, and reveled using DAB. Images show a 20x magnification of cells expressing hAPP (A) and GFP (C) or only GFP (B, D). Scale bar: 20 µm.

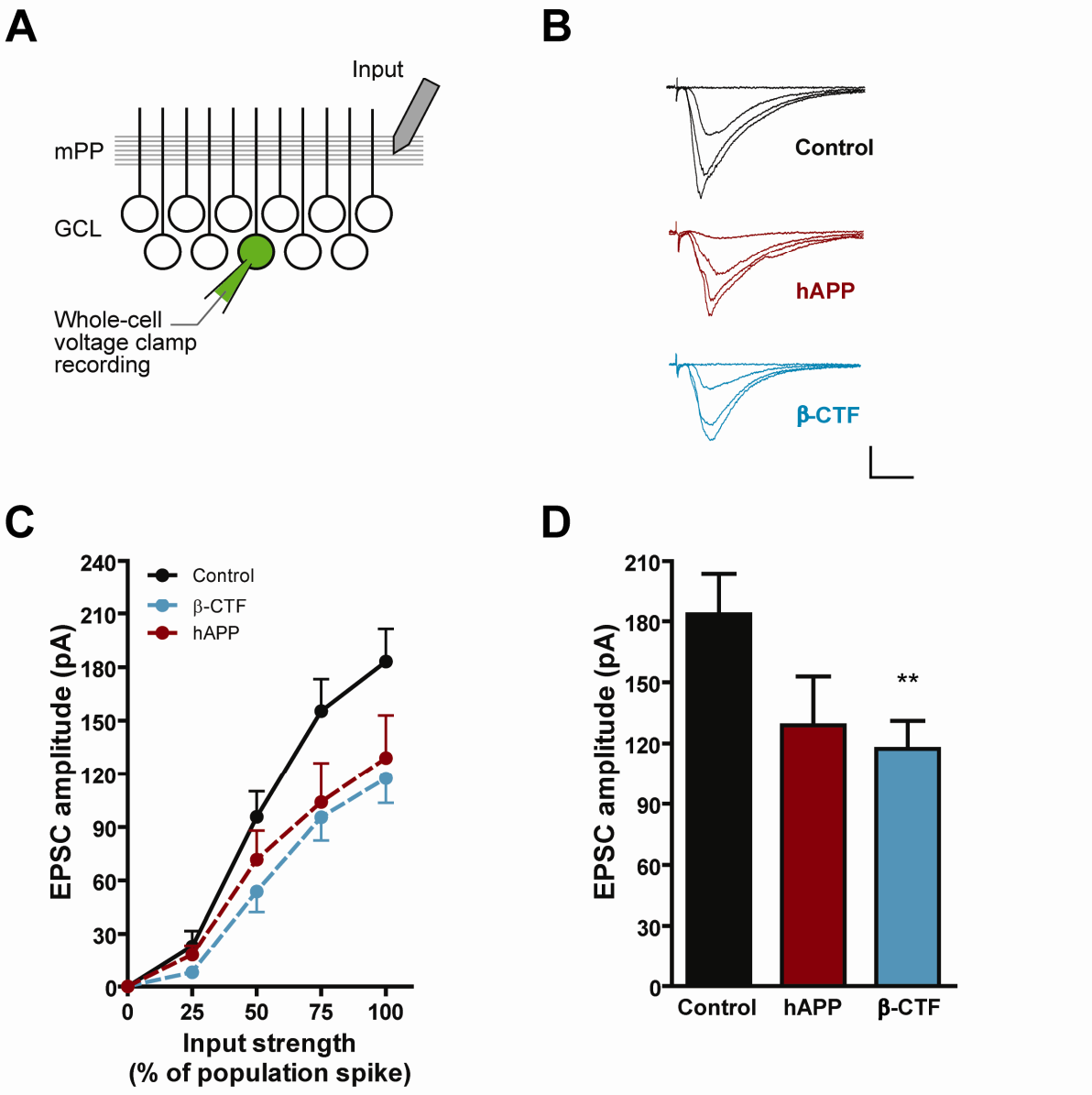

Figure 1

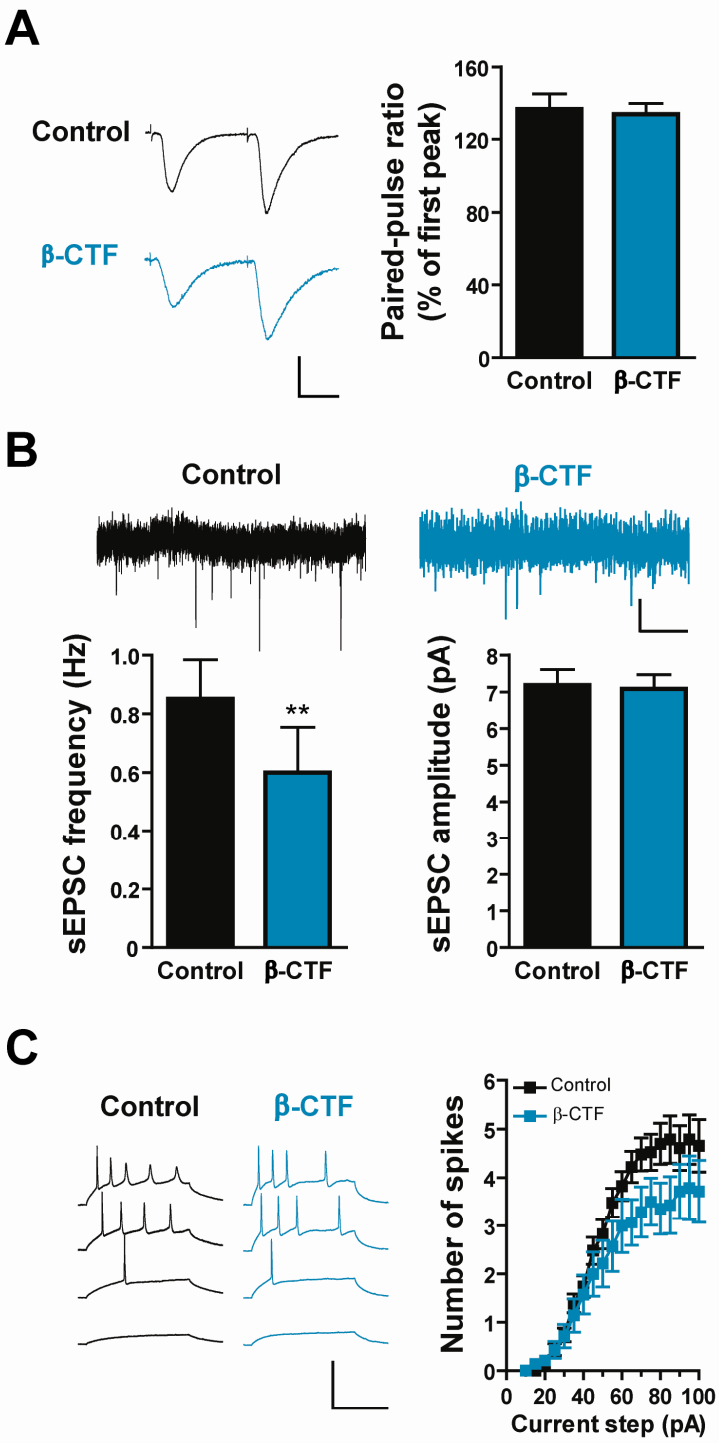

Figure 2

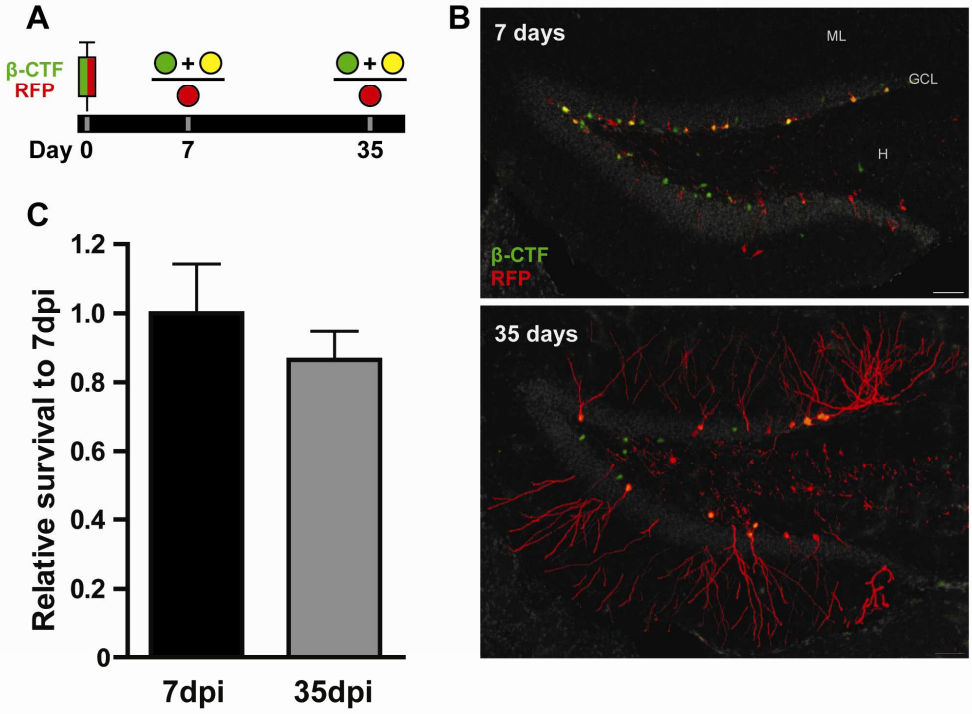

Figure 3

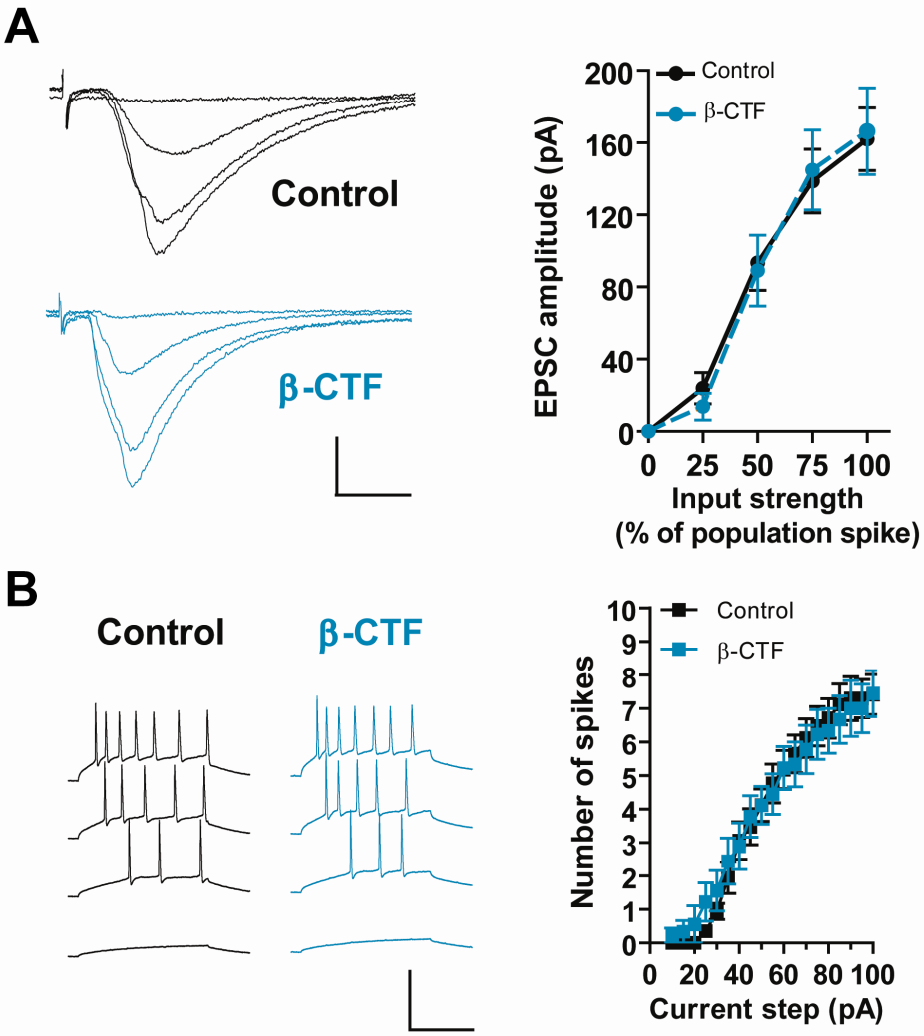

Figure 4

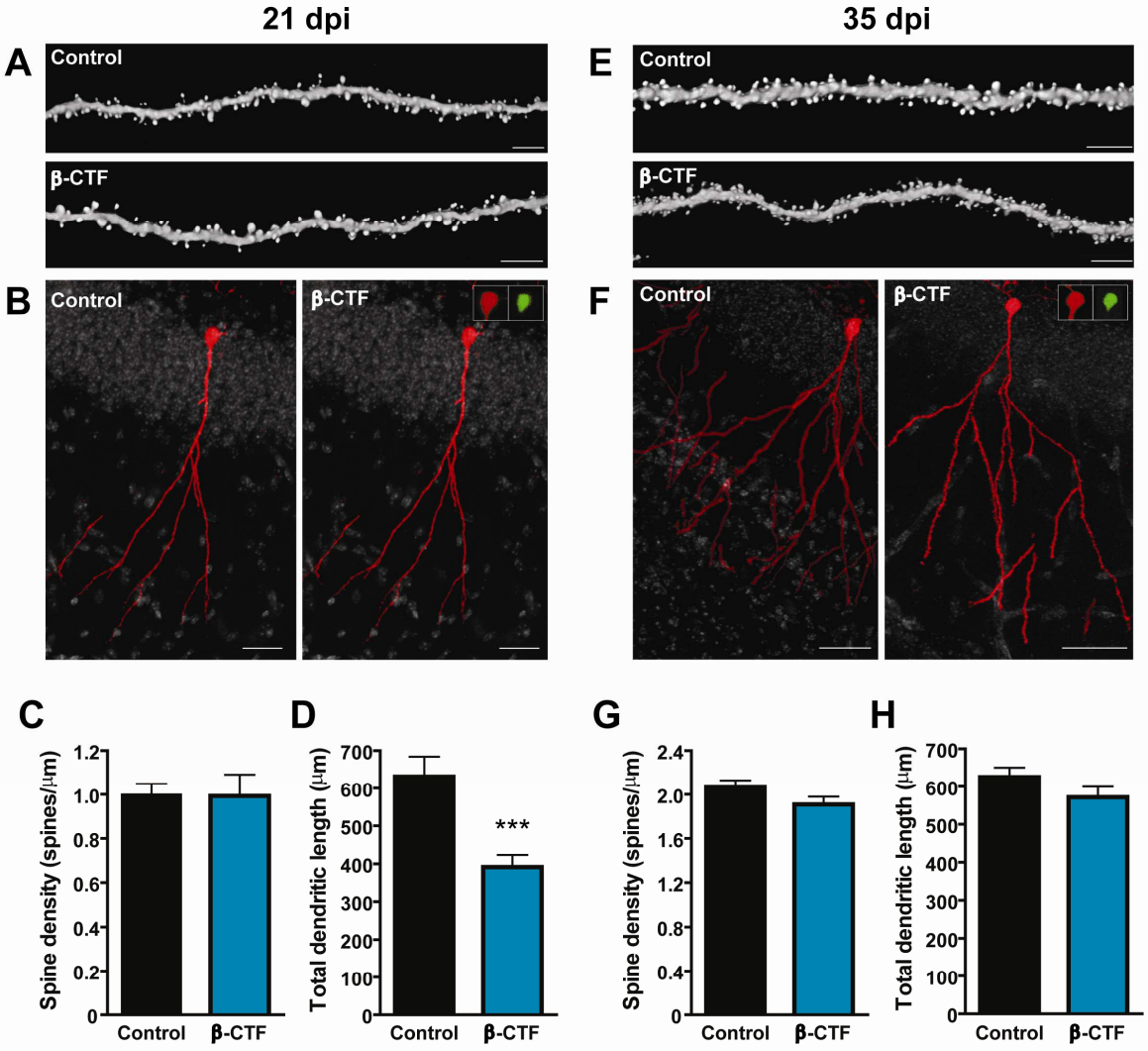

Figure 5

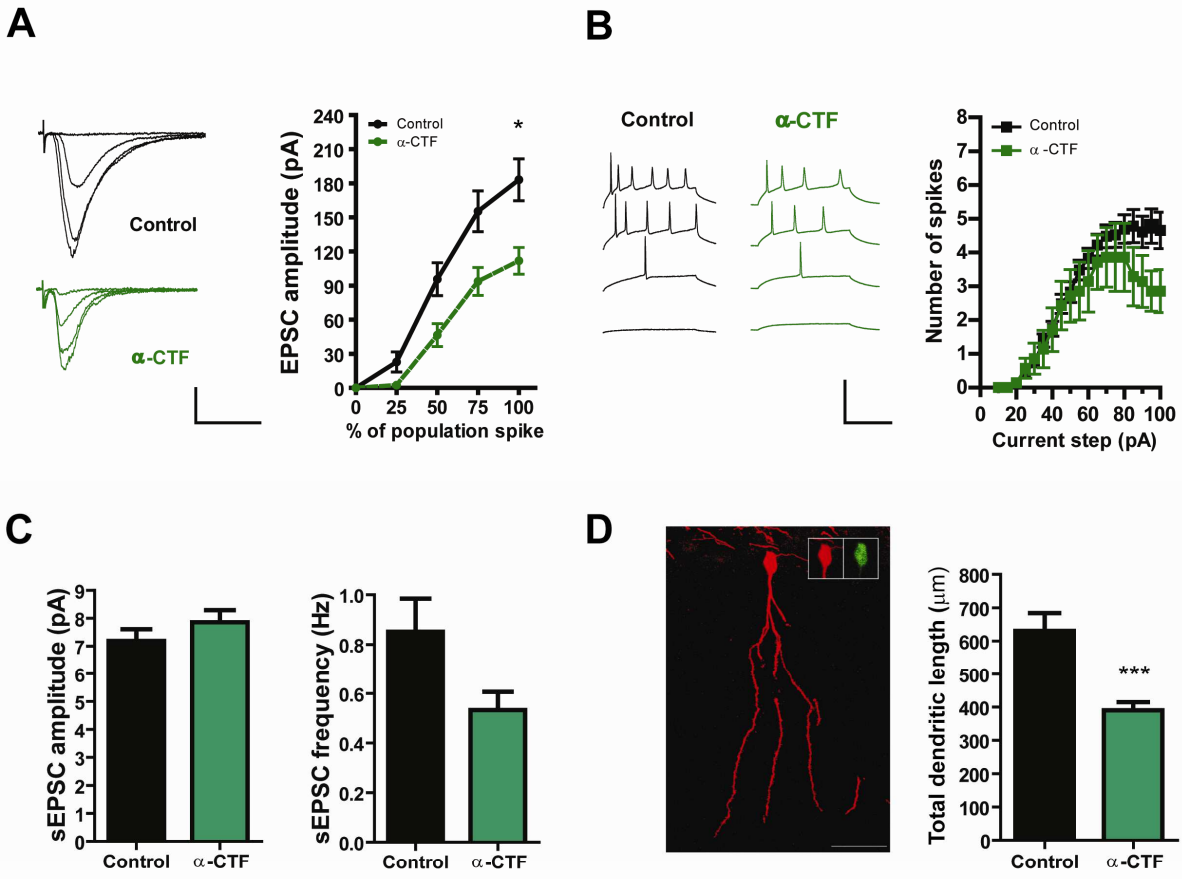

Figure 6

Table 1

		Rinput (GΩ)			Cm (pF)			Vm (mV)			Peak I Na^+ (nA)		
21 dpi	**Control**	1.95 ± 0.28	(20)		47.4 ± 3.6	(20)		-58.1 ± 2.4	(20)		-5.92 ± 0.68	(14)	
	β-CTF	2.04 ± 0.31	(14)		36.8 ± 3.6	(14)		-60.1 ± 3.5	(14)		-4.93 ± 0.79	(14)	
	α-CTF	2.49 ± 0.17	(8)		35.7 ± 1.4	(8)		-42.3 ± 3.2*	(8)		-4.45 ± 0.36	(8)	
35 dpi	**Control**	1.20 ± 0.10	(17)		61.6 ± 2.5	(17)		-68.9 ± 2.2	(17)		-6.88 ± 0.53	(17)	
	β-CTF	1.10 ± 0.10	(10)		55.9 ± 1.5	(10)		-67.0 ± 3.2	(10)		-7.96 ± 0.44	(10)	